Computers and Fluids 173 (2018) 59–72

Contents lists available at ScienceDirect

Computers and Fluids

journal homepage: www.elsevier.com/locate/compfluid

Direct numerical simulation study of hydrogen/air auto-ignition in turbulent mixing layer at elevated pressures

Tong Yao[a], Wen Hao Yang[a], Kai Hong Luo[a,b,*]

[a] Center for Combustion Energy, Key Laboratory for Thermal Science and Power Engineering of Ministry of Education, Department of Thermal Engineering, Tsinghua University, Beijing 100084, China

[b] Department of Mechanical Engineering, University College London, Torrington Place, London WC1E 7JE, UK

ARTICLE INFO

Article history:
Received 1 October 2017
Revised 26 March 2018
Accepted 28 March 2018
Available online 6 April 2018

Keywords:
Direct numerical simulation
Hydrogen
Mixing layers
Ignition
Elevated pressures

ABSTRACT

Auto-ignition of turbulent stratified mixing layer between hydrogen and hot air under elevated pressures $p = 1$–30 atm is studied using direct numerical simulations (DNS) in this work. Homogeneous isotropic turbulence is superimposed on the field. Detailed chemical mechanism and multicomponent diffusion model are employed. Other than turbulent mixing ignition (TMI), homogeneous mixing ignition (HMI) and laminar mixing ignition (LMI) are also investigated for comparison. For both laminar and turbulent cases, the onset of auto-ignition always happens at the same most reactive mixture fraction isosurfaces. Most reactive mixture fractions in diffusion auto-ignition are inconsistent with HMI calculations and shift to the rich side owing to diffusion for all pressures. At elevated pressures, auto-ignition chemistry is different from low pressures. The importance of H_2O_2 and HO_2 is highlighted as radical sinks during the ignition process, and can also be used as an indicator for locating the ignition spots. Moreover, OH radicals can be used as a marker variable for the transition of auto-ignition to flame propagation under high pressures. Two stages are involved in the diffusion ignition process: radical explosion and thermal runaway. According to our study, under elevated pressures, turbulence has little influence on the radical explosion stage. The role of turbulence is to accelerate the thermal runaway stage in the kernels to make the ignition delay time (IDT) shorter than laminar cases.

1. Introduction

Hydrogen as a fuel is promising for its wide inflammable limits, fast burning speeds and zero emissions of carbon dioxide after combustion, and is now used as fuel or fuel additive in practical engines like HCCI [1,2] and gas turbine combustors [3]. Auto-ignition characteristics of hydrogen have been widely studied in homogeneous and laminar unstrained and strained configurations [4,5]. At low temperatures, an inverted "S" shaped curve divides the explosive and nonexplosive regions. At higher pressures, secondary branching involving the formation and decomposition of H_2O_2 characterizes the third explosion limit. Within the explosive region, differences in the nature of the reaction have been experimentally observed in shock tubes as "weak" and "strong" ignition corresponding to a transition around the extended second limit [6].

In practical combustion applications, partially premixed flames in turbulence are ubiquitous. Thus, it is important to study auto-ignition in turbulent fuel-air mixtures in the presence of partial premixing to develop design and operating strategies for engines. However, it is a multifaceted problem and difficult to model for its non-equilibrium features and intrinsic complexity involving chemical reactions, molecular and thermal diffusion, and turbulent transport, especially with presence of compositional stratifications.

Among many applications, DNS has been applied to the study of auto-ignition in turbulent partially premixed mixtures with thermal and/or compositional stratifications [7,8]. Even though this method requires prohibitive numerical costs for practical engineering configurations at large scales, it offers an excellent complement to experiments in order to assess the various physical mechanisms, to obtain complementary information on flame structures, and therefore to improve turbulent combustion modelling. 2D DNSs of non-homogeneous hydrogen–air mixtures with a random initial velocity and mixture fraction fields have been reported by Echekki and Chen [9,10]. Multi-step kinetics were employed to model hydrogen oxidation and simulated pressure was 1 bar.

Auto-ignition in the turbulent mixing layer is one of the canonical partial premixing configurations. Hot spots form locally in the lean mixture zone with heat release and temperature increasing.

* Corresponding author at: Department of Mechanical Engineering, University College London, Torrington Place, London WC1E 7JE, UK.
E-mail address: k.luo@ucl.ac.uk (K.H. Luo).

https://doi.org/10.1016/j.compfluid.2018.03.075

The hot spot then propagates toward the stoichiometric isolevel, implying both premixed and non-premixed combustion regimes [11]. The importance of partially premixed combustion during this process has been emphasized in previous work [12]. Mastorakos et al. have reported results from 2D direct numerical simulations (DNS) of methane–air mixing layers in an isotropic homogeneous decaying turbulent environment at elevated initial fuel–air temperatures (approximately 1000–1200 K). A single-step global reaction chemistry mechanism was employed to model methane oxidation. The simulated pressure was 1 bar. They observed that auto-ignition occurred along the 'most reactive' mixture fraction isoline with low magnitudes of the scalar dissipation rate in the fuel–air mixing layer. Higher values of scalar dissipation led to heat and species loss from the reactive regions, thereby delaying auto-ignition.

However, hydrogen's ignition characteristics are markedly different from hydrocarbons like methane. Hydrogen has a very high diffusivity, which results in preferential diffusion, altering global combustion characteristics such as heat release rate, turbulent flame speed and burning rate via thermal-diffusive instabilities [13]. The effects of differential diffusion were investigated by Hilbert and Thevenin [14] and the importance of using detailed diffusion model was emphasized. 2D DNS of auto-igniting hydrogen–air mixtures in an isotropic homogeneous decaying turbulence have also been reported by Im et al [15]. Multi-step kinetics were employed to model hydrogen–air oxidation. The initial temperatures of the fuel and air streams were selected to be 1100 K and 300 K respectively, and simulated pressure was 1 bar. Im et al. [15] considered constant Lewis numbers for each species. Thermal diffusion was not considered. Hilbert and Thevenin [16] investigate auto-ignition of hydrogen/air mixing layer using different diffusion model including Le number equals to unity, constant Lewis numbers for each species and multi-component diffusion model. They found that the onset of heat release is influenced by the diffusion.

However, previous DNS studies of auto-ignition of hydrogen/air mixing layer mentioned above were performed in high temperatures or low pressures which lie in the regime of strong ignition. The role of elevated pressure is not well demonstrated, especially with detailed chemical kinetics and multi-component transport models. At high pressures, ignition delay time becomes much longer than atmospheric condition. Investigation of ignition problems of high pressures leads to much more computational cost, which is not feasible in previous studies. In the present work, direct numerical simulations are employed to investigate a time-dependent H_2/N_2/air igniting mixing layer using detailed models for chemistry and diffusion velocities under stepping-up pressures from 1 atm to 30 atm. As pressures increase, auto-ignition falls into weak ignition regime, in which auto-ignition delay time becomes longer. The ignition chemistry of high pressures is much different from that of low pressures and interacts with turbulence intricately. The aim of this paper is to provide a better understanding of auto-ignition in thermally and compositionally stratified hydrogen/air mixtures using DNS under elevated pressures.

2. Numerical methods

A DNS must resolve both fluid dynamics and flame structures, especially for the non-equilibrium auto-ignition process. Even though this method requires prohibitive computational costs for practical engineering configurations, it offers an excellent complement to experiments in order to assess the importance of various physiochemical mechanisms, to obtain complementary information on flame structures, and therefore to improve turbulent combustion modelling.

Turbulent auto-ignition process in the present study is governed by the Navier–Stokes equations, the continuity equation, and the transport equations for energy and species mass fractions. The body force, the Soret effects and the radiation heat transfer are neglected. A DNS code Parcomb [17] is used to solve these equations.

$$\frac{\partial \rho}{\partial t} + \frac{\partial \left(\rho u_j\right)}{\partial x_j} = 0$$

$$\frac{\partial \left(\rho u_i\right)}{\partial t} + \frac{\partial \left(\rho u_i u_j\right)}{\partial x_j} = -\frac{\partial p}{\partial x_i} + \frac{\partial \tau_{ij}}{\partial x_j}$$

$$\frac{\partial \left(\rho Y_k\right)}{\partial t} + \frac{\partial \left(\rho u_j Y_k\right)}{\partial x_j} = -\frac{\partial \left(\rho Y_k V_{kj}\right)}{\partial x_j} + \dot{\omega}_k,\ k = 1,\ 2, \ldots, N_s$$

$$\frac{\partial \left(\rho e_t\right)}{\partial t} + \frac{\partial \left(\rho u_j e_t + p u_j\right)}{\partial x_j} = -\frac{\partial q_j}{\partial x_i} + \frac{\partial \left(\tau_{ij} u_i\right)}{\partial x_j}$$

$$\frac{p}{\rho} = \frac{R}{\bar{W}} T$$

where ρ represents mixture density, u_j the components of velocity, p the pressure, N_s the total number of species, V_{kj} the component of the diffusion velocity of species k in the direction of j, $\dot{\omega}_k$ the chemical production rate of species k, q_j the jth component of the heat flux vector and τ_{ij} the stress tensor:

$$\tau_{ij} = \eta \left[\frac{\partial u_i}{\partial x_j} + \frac{\partial u_j}{\partial x_i}\right] - \frac{2}{3}\eta \frac{\partial u_k}{\partial x_k}\delta_{ij}$$

where δ_{ij} is the Kronecher symbol and η is the dynamic viscosity.

The detailed description of the code has been reported in several previous studies [17–20] and will be briefly described here. A spatial sixth-order central scheme and an explicit fourth-order Runge-Kutta time integrator are employed. In its recent version [18–20], the skew-symmetric formulation [21] has been implemented for the convective terms in order to reduce even further numerical dissipation and increase stability. The formulation is high order and contains no artificial dissipation. Numerical stability is enhanced through semi-discrete satisfaction of global conservation properties stemming from the second law of thermodynamics and the entropy equation. The numerical implementation is achieved using a conservative skew-symmetric splitting of the nonlinear terms. The extended Navier-Stokes Characteristic Boundary Conditions (NSCBC) [22,23] are used, with pressure relaxation applied along all open faces. The accuracy of the code has been assessed in several previous studies [16,24–28].

The parallelization is in a 3D block structure using the MPI protocol for data exchange. The code offers a good peak performance and a near perfect parallel scaling for up to 4096 computing cores on ARCHER. Furthermore, a fully parallel I/O (via MPI-I/O) is employed in the code, where multiple processes of the parallel program access data (for read/write) from a common, shared file. This technique provides both higher performance (speedup in time needed for writing/reading all files by a factor of at least 3 compared with sequential I/O) and single (restart/solution) data files.

3. Computational configurations

The DNS domain is two-dimensional with periodic and subsonic non-reflecting boundary conditions. The domain size is 1 cm × 1 cm. On the left, we impose $T = 1100$ K, $Y_{O2} = 0.233$ and $Y_{H2} = 0$. On the right of the domain, we have $T = 300$ K, $Y_{O2} = 0$, and $Y_{H2} = 0.023$. An appropriate nitrogen complement is then added, and initial velocities are set equal to zero. The initial domain and conditions are shown in Fig. 1. The mixing layer in temperature and species between air and fuel is imposed as hyperbolic-tangent profiles with a stiffness parameter. The initial values for any primitive variable e.g. mixture fraction ξ are transformed into smooth profiles according to:

$$\xi = \frac{1}{2}[1 - tanh(s \cdot (x - x_m))]$$

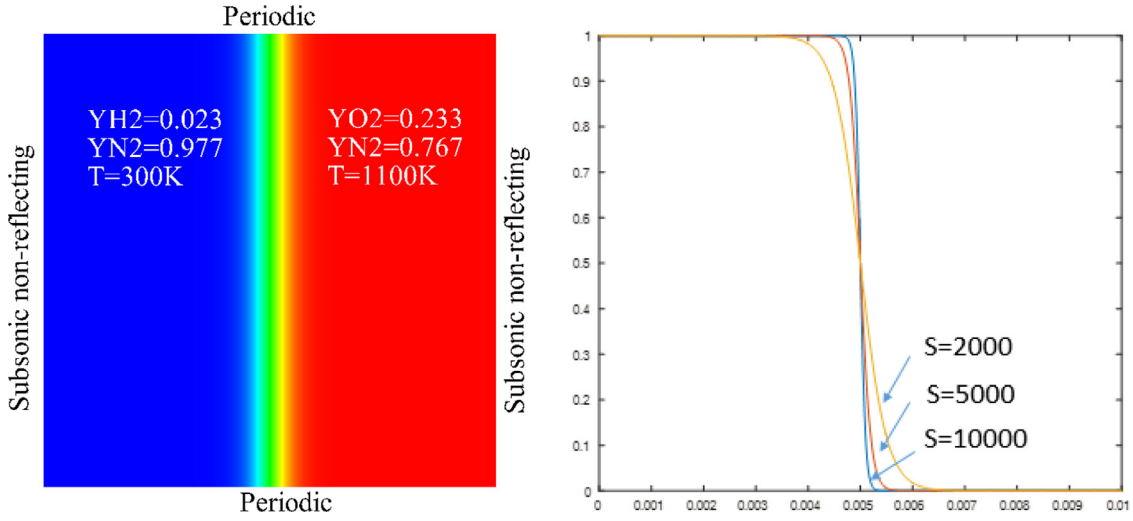

Fig. 1. The computational domain and initial mixing layer distributions.

Table 1
Turbulence conditions for calculations.

p (atm)	u' (m/s)	l_t (mm)	τ_t (ms)	Re_t	η (μm)	Grid	Resolution (μm)	Cost (cpu • hours)
1	1.6	1.6	1.0	148	38	1000^2	10	1,200
5	0.72	0.72	1.0	148	17	2000^2	5	20,160
10	0.5	0.5	1.0	148	12	2000^2	5	28,800
30	0.29	0.29	1.0	148	7	5000^2	2	720,000

where x_m is the middle of the x axis. The constant s is a measure of the stiffness at the fresh/burnt gas interface. The initial profiles of mixture fraction with different stiffness are shown in Fig. 1 (on the right side). The present study uses the stiffness of $s = 2000$.

Turbulent conditions for different pressures investigated in the present study are listed in Table 1. Turbulent intensity u' and integral length scale l_t are set to characterize turbulence. Turbulent time scale τ_t and turbulent Reynolds number Re_t are kept identical for different pressures. Turbulent time scale τ_t is 1 ms, and the turbulent Reynolds number Re_t is 148. Kolmogorov scales η are calculated to determine the spatial resolution of the computational domain. 1001×1001 grids, 2001×2001 grids, 2001×2001 grids, 5001×5001 grids are used and allow spatial resolutions of 10 μm, 5 μm, 5 μm, 2 μm for pressures $p = 1$ atm, 5 atm, 10 atm, 30 atm respectively. Kolmogorov scales (η) are resolved by 3 grids which are adequate for convergence [31]. Time step is controlled by the CFL number.

A detailed chemical scheme of nine species (H_2, O_2, H_2O, OH, H, O, HO_2, H_2O_2, and N_2) and 37 reactions to describe the combustion of H_2 in the air [29] is included, taking into account multicomponent diffusion velocities and thermo-diffusion effects. Thermo-dynamic parameters are determined using fifth-order polynomial fits of experimental measurements. A field of homogeneous isotropic pseudo-turbulence is superimposed on initial profiles at $t = 0$. The parameters chosen by the user are the root-mean-square (RMS) velocity u' which indicates the turbulent intensity and the integral length-scale of turbulence.

Mixture fraction ξ characterizes the level of mixing between the reactants. It takes a value of 0 in pure oxidizer and a value of 1 in pure fuel. A careful definition of the mixture fraction ξ is required when taking into account differential diffusion. The following formulation, proposed in [30] and has been checked for various configurations, is used in the present work:

$$\xi = \frac{(Y_H - Y_{H,ox})/2W_H - (Y_O - Y_{O,ox})/W_O}{\left(Y_{H,fu} - Y_{H,ox}\right)/2W_H - \left(Y_{O,fu} - Y_{O,ox}\right)/W_O}$$

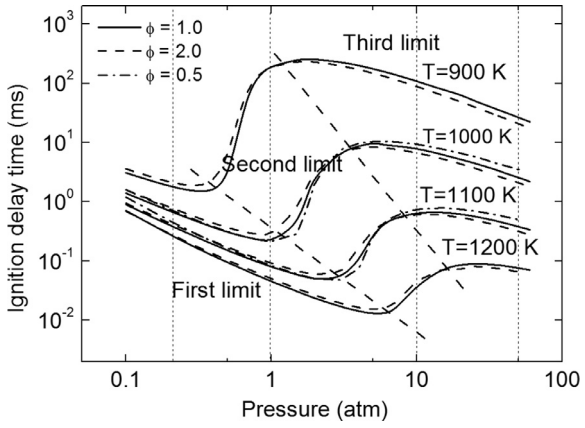

Fig. 2. Homogeneous auto-ignition delay time versus pressure under various initial temperatures $T = 900$–1200 K and equivalence ratios $\varphi = 0.5$–2.0.

where Y_H and Y_O are the elemental mass fractions of elements H and O, and the subscript ox and fu stand for initial conditions on, respectively, the oxidizer and fuel sides. W_H and W_O stand for relative elemental mass for H and O.

In mixture fraction space

$$\frac{\partial \emptyset}{\partial t} = \frac{\chi}{2}\frac{\partial^2 \emptyset}{\partial Z^2} + \frac{\dot{\omega}}{\rho}$$

χ is the instantaneous scalar dissipation rate defined as

$$\chi = 2D(|\nabla \xi|)^2$$

4. Results and discussion

4.1. Homogeneous mixing ignition

Homogeneous mixing ignition (HMI) is the simplest model to study the chemical kinetics effects on ignition leaving out of con-

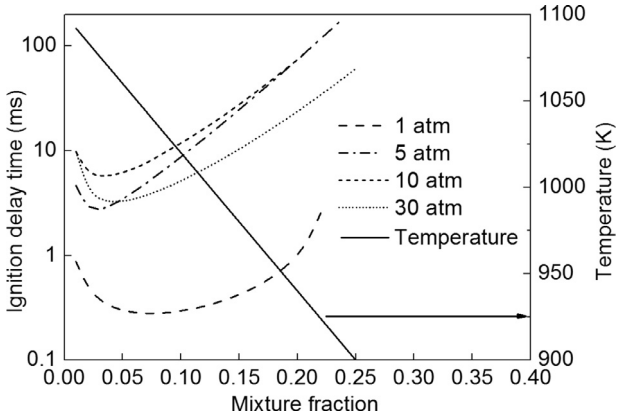

Fig. 3. Auto-ignition delay time in HMI versus mixture fraction under various pressures $p = 1$, 5, 10, 30 atm.

vection and diffusion. Before investigating more complicated auto-ignition problems in the turbulent mixing layer, homogeneous auto-ignitions of hydrogen/air pre-mixture are performed first using zero-dimensional code SENKIN [32] under various pressures, temperatures and compositions. As the ignition delay time (IDT) is characterized by a period of radical build-up and the following heat release with temperature increasing. IDT t_{ign} can be defined by Eq. (1) as the instant of inflection point of maximum heat release rate q_{max}.

$$\frac{\partial^2 q_{\max}}{\partial t^2}\Big|_{t=t_{ign}} = 0 \tag{1}$$

IDTs are measured and plotted versus pressures in Fig. 2. It can be seen that in the temperature range of T = 900–1200 K, IDT decreases with temperature increasing, and IDT is not as sensitive to equivalence ratio as to temperature. It is worth noting that IDT changes with pressure non-monotonically. IDT decreases first and then increases following by slowly decreasing as pressure increases along a fixed temperature line. As pressure increases, ignition falls to different ignition limit regime characterized by different chemical kinetics and reaction paths, which will be demonstrated later. The first ignition limit is identified as the low-pressure region where the IDT drops with increasing pressure. In the second ignition limit, IDT rises as pressure increases. In addition, in the third limit, IDT decreases slowly with pressure increasing. Representative pressures $p = 1$, 5, 10, 30 atm in different ignition regimes are selected to perform further studies on diffusion auto-ignition (Fig. 2).

HMI technique can be used as a simple model to investigate auto-ignition in the mixing layer without diffusion. A batch of HMI samples is performed with different temperatures and compositions under a specific pressure. Each sample of HMI can be treated as an ignition location isolated from its neighbours and left to ignite. The initial profiles of mass fractions of reactants and temperature can be interpreted by the mixture fraction as follows, IDT of each sample then can be characterized by its mixture fraction ξ

$$\begin{aligned} Y_H &= Y_{H,fu}\xi \\ Y_O &= Y_{O,ox}(1-\xi) \\ T &= T_{ox} - \xi\left(T_{ox} - T_{fu}\right) \end{aligned}$$

where $Y_{H,\,fu} = 0.023$, $Y_{O,\,ox} = 0.233$, $T_{ox} = 1100$ K, $T_{fu} = 300$ K. IDTs t_{ign} of each sample are plotted as a function of ξ in Fig. 3. The temperature profile is also shown. For all cases under different pressures, IDT decreases from the very lean mixtures to the richer side, then a minimum IDT occurs and most-reactive mixture fraction

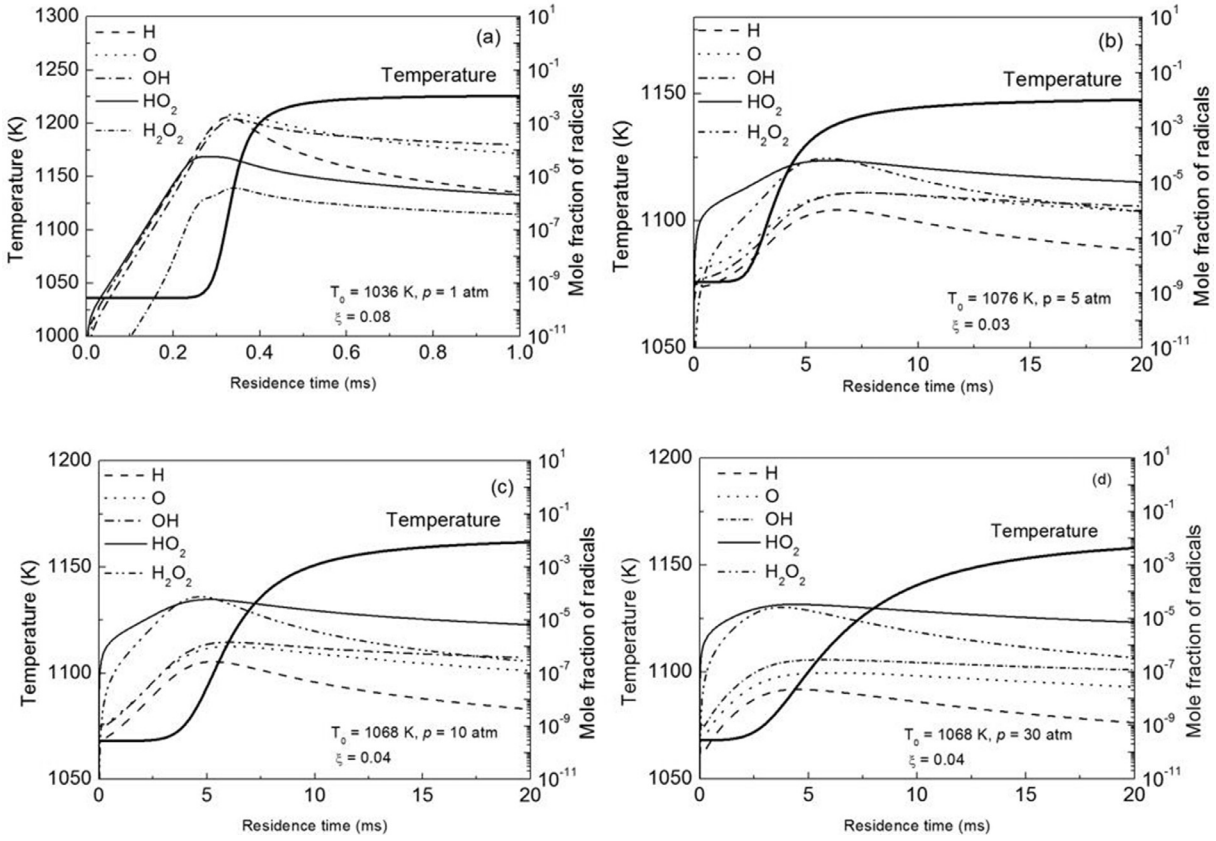

Fig. 4. Evolution of temperature and radicals in HMI corresponding to the most reactive mixture fraction under different pressures (a) $p = 1$ atm (b) $p = 5$ atm (c) $p = 10$ atm (d) $p = 30$ atm.

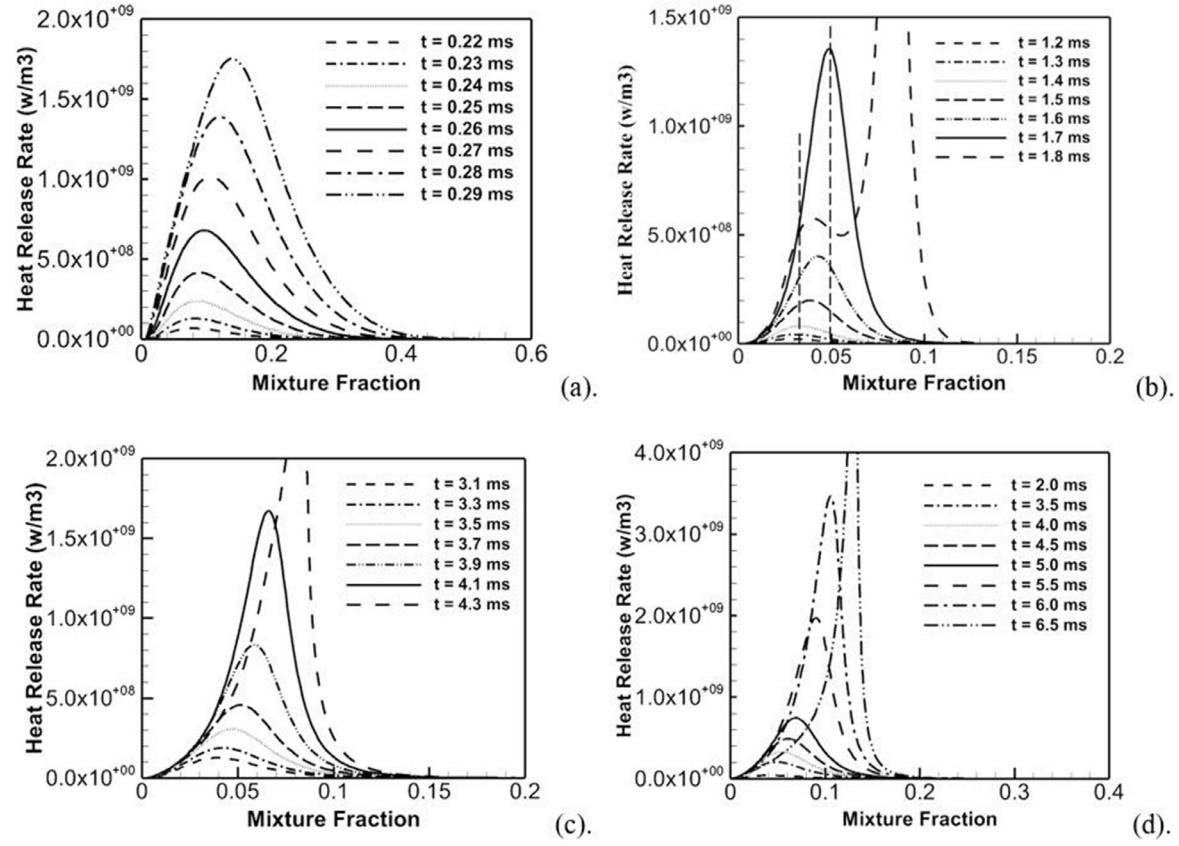

Fig. 5. LMI calculation: instantaneous value of the local heat release as a function of the mixture fraction under different pressures (a) $p = 1$ atm (b) $p = 5$ atm (c) $p = 10$ atm (d) $p = 30$ atm.

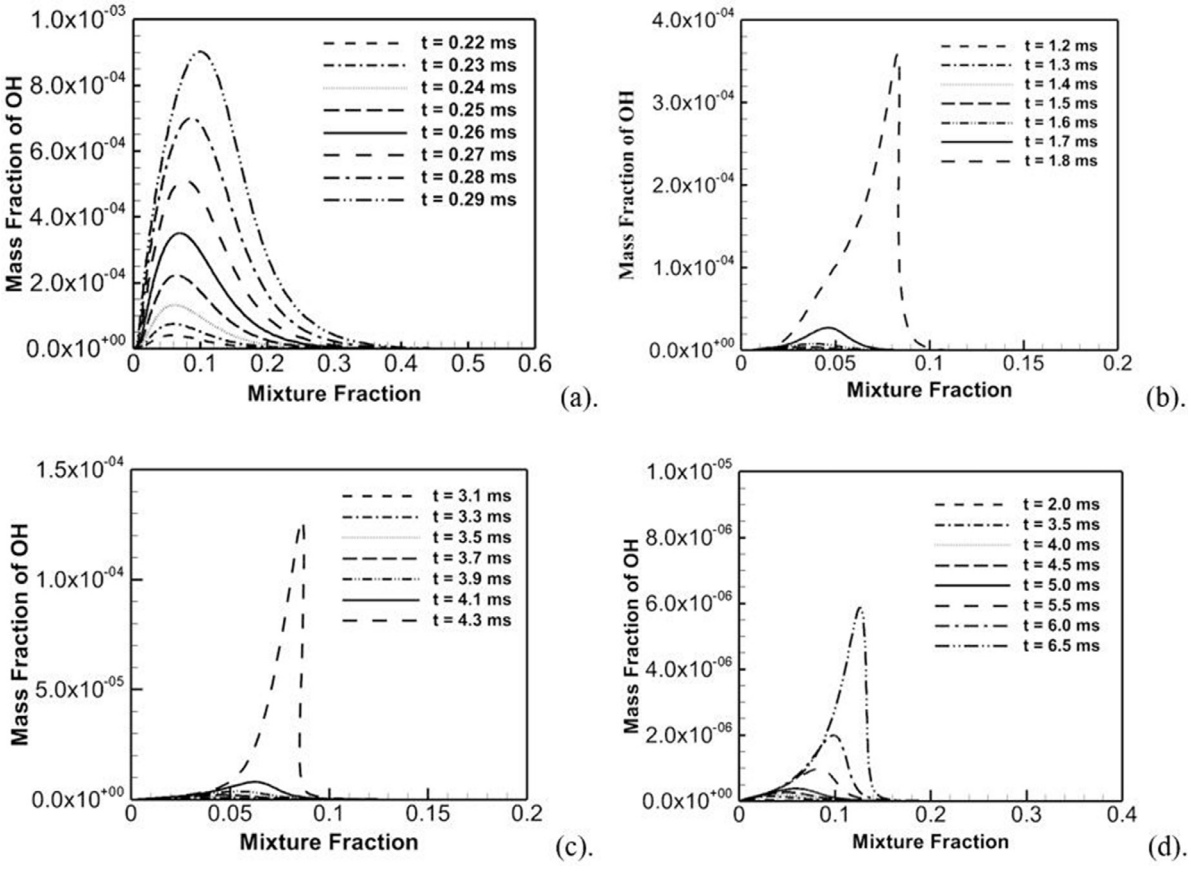

Fig. 6. LMI calculation: instantaneous value of the local OH radical mass fraction as a function of the mixture fraction under different pressures (a) $p = 1$ atm (b) $p = 5$ atm (c) $p = 10$ atm (d) $p = 30$ atm.

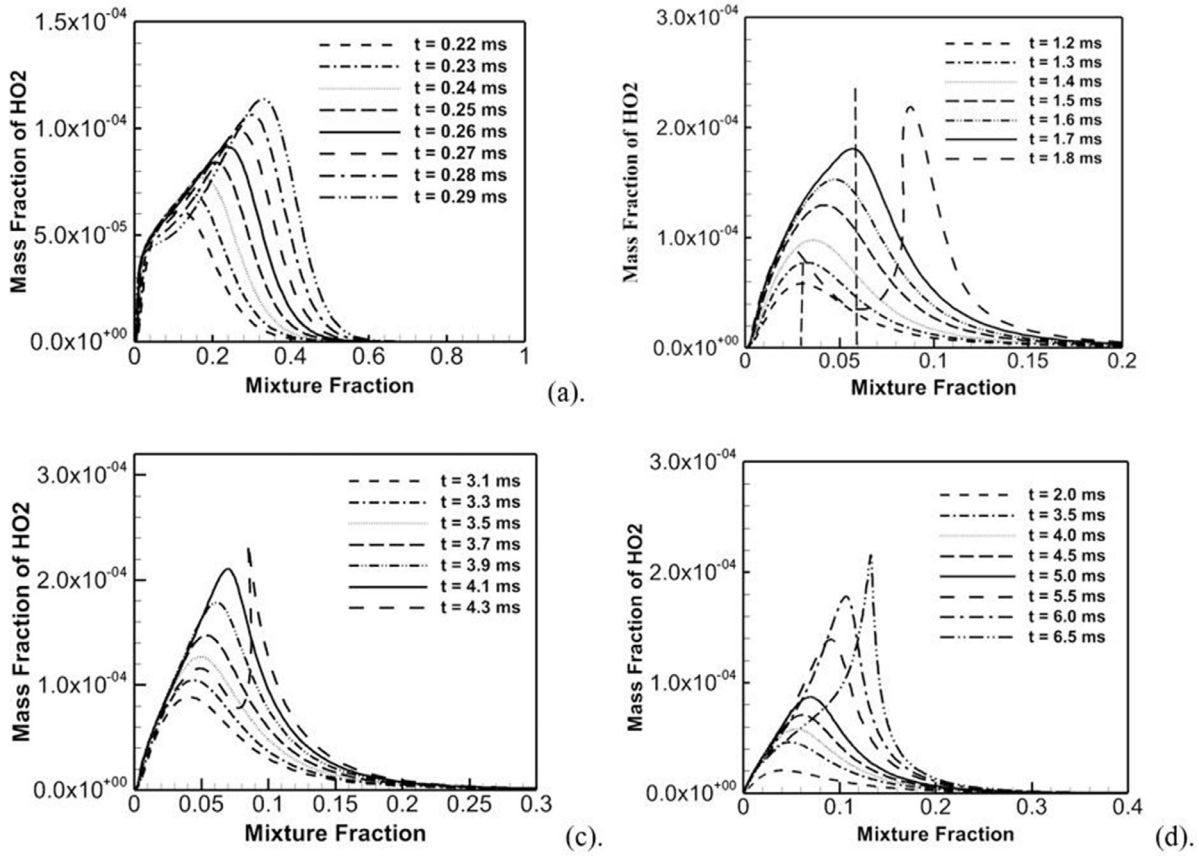

Fig. 7. Laminar mixing ignition (LMI) calculation: instantaneous value of the local HO_2 radical mass fraction as a function of the mixture fraction under different pressures (a) $p = 1$ atm (b) $p = 5$ atm (c) $p = 10$ atm (d) $p = 30$ atm.

ξ_{mr} which corresponds to the minimum of ignition delay times can be found. The most reactive mixture fraction still locate in the lean mixtures. At high values of mixture fraction, IDT increases and shows an almost exponential behaviour. Most reactive mixture fractions are 0.08, 0.03, 0.04, 0.04 for pressures $p = 1$, 5, 10, 30 atm, respectively. The IDTs of different pressures are consistent with the previous ignition regime (Fig. 2) overall.

Most reactive mixture fractions obtained by HMI was used as an indicator of positions in the mixture fraction space for the onset of auto-ignition in laminar and turbulent diffusion flames in previous studies [9–11]. However, the isolated ignition assumption in mixing layer is not adequate in practical cases, as diffusion may play an important role in this process and influence the auto-ignition locations in the mixture fraction space, which will be shown later.

Fig. 4 shows the evolution of temperature and radicals during the HMI process corresponding to the most reactive mixture fraction ξ_{mr} under different pressures. For all cases, auto-ignition process can be divided into two stages. The first is induction stage characterized by a radical explosion without heat release, and radicals accumulate quickly without temperature increase. The second stage is thermal runaway characterized by the temperature increase to final equilibrium. It can be seen that radicals behave differently in the induction stage for low and high pressures.

Fig. 4(a) shows the evolution of radicals and temperature during the ignition process at $p = 1$ atm, which belongs to the first ignition limit. It can be seen that concentrations of all radicals increase exponentially in the induction stage before noticeable temperature rising. Concentrations of HO_2 and H_2O_2 drops slightly then and their peaks locate at the onset of temperature increasing stage. Radicals of H, O, OH continues to increase exponentially and reach their peak concentrations at the ignition instant. Therefore, H radicals could be used as a good candidate of marker variable of the ignition delays under pressure $p = 1$ atm.

As pressure increases to $p = 5$ atm, it can be seen in Fig. 4(b) that HO_2 and H_2O_2 play more prominent roles and the peak concentrations of HO_2 and H_2O_2 radicals are two orders of magnitude more than that of H radical. Concentrations of HO_2 and H_2O_2 radicals increase dramatically at the very beginning, and the growth slows down until the ignition point. Although the concentration of H radicals grows almost exponentially in the induction stage, the slope of growth along with the peak concentration is far less than that at $p = 1$ atm, which leads to a much longer ignition delay time. Elementary reactions analysis shows that in the very early stage of ignition, the radical pool is initiated by slow reaction between H_2 and O_2 through $H_2 + O_2 = H + HO_2$. HO_2 further accumulates through $H + O_2 + M = HO_2 + M$ and acts as a "sink" along with H_2O_2 for other radicals like H, O, OH. Chain branching reaction $HO_2 + H = OH + OH$ which consumes HO_2 becomes increasingly important as the temperature begins to increase and the ignition instant is approaching.

Profiles of temperature and radicals concentrations during auto-ignition process at $p = 10$ atm are shown in Fig. 4(c). As crossover pressure between the second and third ignition limits, evolutions of radicals are almost identical to that of $p = 5$ atm. Although radicals reach peak concentration earlier than $p = 5$ atm, ignition delay time is longer.

Fig. 4(d) shows temperature and radicals evolution at $p = 30$ atm. Although induction time for radicals accumulation decreases, thermal runway time becomes longer, which is caused by moderate heat release. It is worth noting that peak concentration of HO_2 before ignition reaches the same level and corresponds

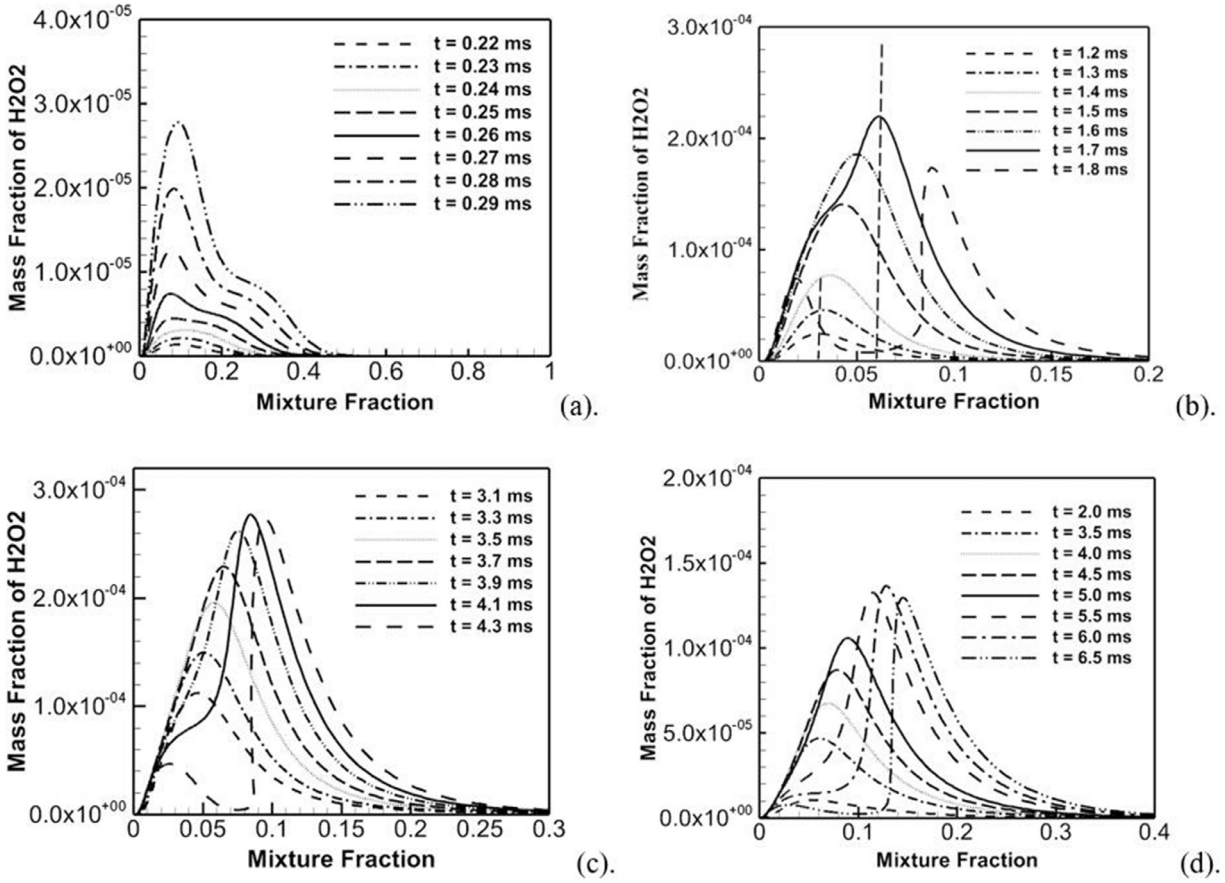

Fig. 8. LMI calculation: instantaneous value of the local H_2O_2 radical mass fraction as a function of the mixture fraction under different pressures (a) $p = 1$ atm (b) $p = 5$ atm (c) $p = 10$ atm (d) $p = 30$ atm.

to a mass fraction of 10^{-4} for different pressures. The value of HO_2 peak concentration can be used as a better indicator of onset of ignition than H radicals at elevated pressures.

4.2. Laminar mixing ignition

As diffusion is supposed to play an important role in the auto-ignition process of mixing layer, laminar mixing ignition (LMI) model is employed to accounts for diffusion in one-dimension. Detailed multicomponent transport formation is used to accurately predict preferential diffusion effects in the hydrogen flame. IDT is defined as the period from $t = 0$ ms to the instant of inflection of maximum heat release rate in the domain. The defined of IDT in LMI is consistent with HMI.

The instantaneous values of local heat release in the mixture fraction space around the auto-ignition under different pressures of LMI calculations are shown in Fig. 5. IDTs for different pressures are 0.28, 1.7, 4.1, 6.0 ms, respectively. The auto-ignition zones are “thinner” for higher pressures because the bottom zone in the vicinity of the most reactive mixture fraction is wider for $p = 1$ atm than others in the HMI calculation shown in Fig. 3. The mixture fraction corresponding to the maximum heat release at the ignition time is most reactive mixture fraction. As pressure increase, the most reactive mixture fractions are 0.11, 0.05, 0.06 and 0.10 for $p = 1$, 5, 10, 30 atm, respectively.

It can be seen from Fig. 5 that ignition spots propagate to the neighbouring rich mixtures and evolve into a flame front after auto-ignition, and heat release rate of the auto-ignition kernels begins to drop for the depletion of the reactants after ignition. Mixture fractions at the very beginning of thermal runway t = 1.2 ms and auto-ignition instant $t = 1.7$ ms are marked with dash lines in Fig. 5(b). Although the onset of thermal runaway locates at the mixture fractions identical to HMI, the most reactive mixture fraction is inconsistent with the homogeneous calculation and shift to the rich side because of diffusion. It is the same for other pressures. Therefore, identification of the most reactive mixture fraction using HMI model is insufficient for diffusion auto-ignition.

Although ignition delay time is shorter for $p = 30$ atm than $p = 10$ atm in HMI calculations, diffusion auto-ignition delay time becomes longer. It may be caused by relatively longer thermal runaway time at $p = 30$ atm shown in Fig. 5(d). Heat loss of the ignition spots by diffusion delays the ignition time. Heat release rate reaches about 1.5 GW for $p = 1$, 5 and 10 atm in Fig. 5(a)–(c), it can be seen from Fig. 5(d) that heat release rate of $p = 30$ atm is doubled at the ignition time compared with other cases.

Fig. 6 shows the instantaneous value of the local OH mass fraction in the mixture fraction space. It can be seen that OH behaves differently between $p = 1$ am and elevated pressures. The concentration of OH is trivial during auto-ignition at high pressures of the second and third ignition limit zone, which is consistent with the HMI calculations. However, after ignition kernels successfully ignite the neighbourhood and turn into a propagating flame front, mass fractions of OH increases dramatically. Therefore, OH radicals can be used as a marker variable for the transition of auto-ignition to flame propagation, and a global ignition capability of the overall flow at elevated pressures of the second and third ignition zone.

Fig. 7 shows the instantaneous value of the local HO_2 radical mass fraction as a function of the mixture fraction Z under different pressures. Ignition happens instantly after the HO_2 mass reaches the value of 2×10^{-4} except for $p = 1$ atm, which is con-

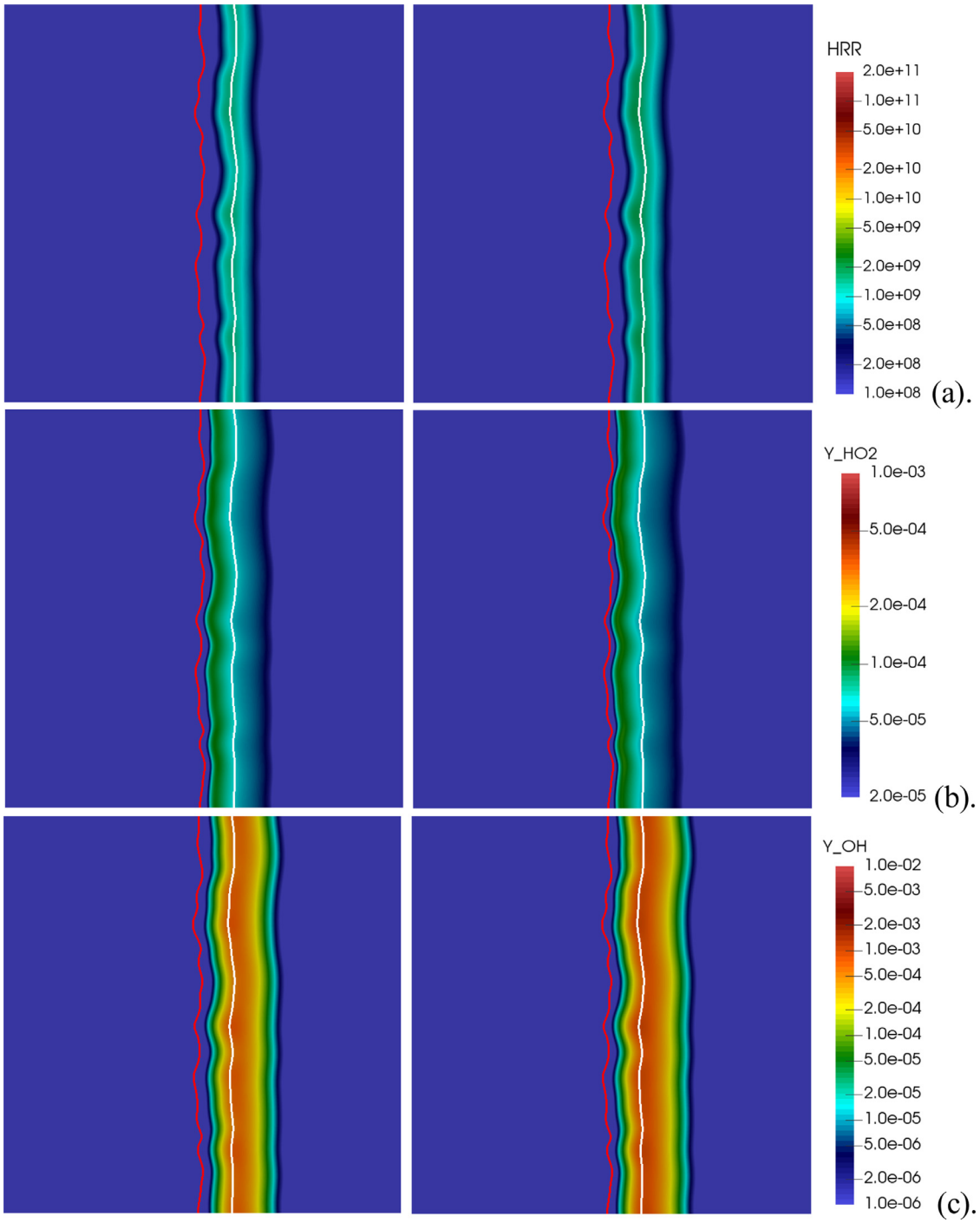

Fig. 9. Turbulent calculation: instantaneous radicals and heat release rate contours at the ignition time for $p = 1$ atm (a) Heat release rate (b) OH (c) HO_2. (For interpretation of the references to colour in this figure text, the reader is referred to the web version of this article.)

sistent with previous study [9]. At the ignition spot, HO_2 is consumed after onset of the auto-ignition. The location of peak HO_2 always remains at lower temperatures. Thus, HO_2 can also be used as an indicator for locating the ignition spots. Most reactive mixture fraction of 0.03 calculated in HMI and 0.06 in LMI are marked with dash lines in Fig. 7(b). It can be seen that peak concentration of HO_2 forms in the mixture fraction of 0.03 (most reactive mixture fraction of HMI) at the early stage of the ignition process but moves to the richer mixture faction subsequently. Peak concentration of HO_2 locates at most reactive mixture fraction of 0.06 and begins to drop after the ignition instant.

Fig. 8 shows the H_2O_2 concentrations at various time instants during the auto-ignition process. At $p = 1$ atm, peak mass fraction of H_2O_2 at ignition instant is $\sim 2 \times 10^{-5}$, which is lower than higher pressures. In Fig. 8(b), at $p = 5$ atm, H_2O_2 reaches peak concentration in the ignition spot which is corresponding to most reactive mixture fraction 0.06 at $t = 1.7$ ms. After ignition, H_2O_2 is almost consumed completely in the ignition spot. Most reactive mixture fraction of 0.03 calculated in HMI and 0.06 in LMI are also marked

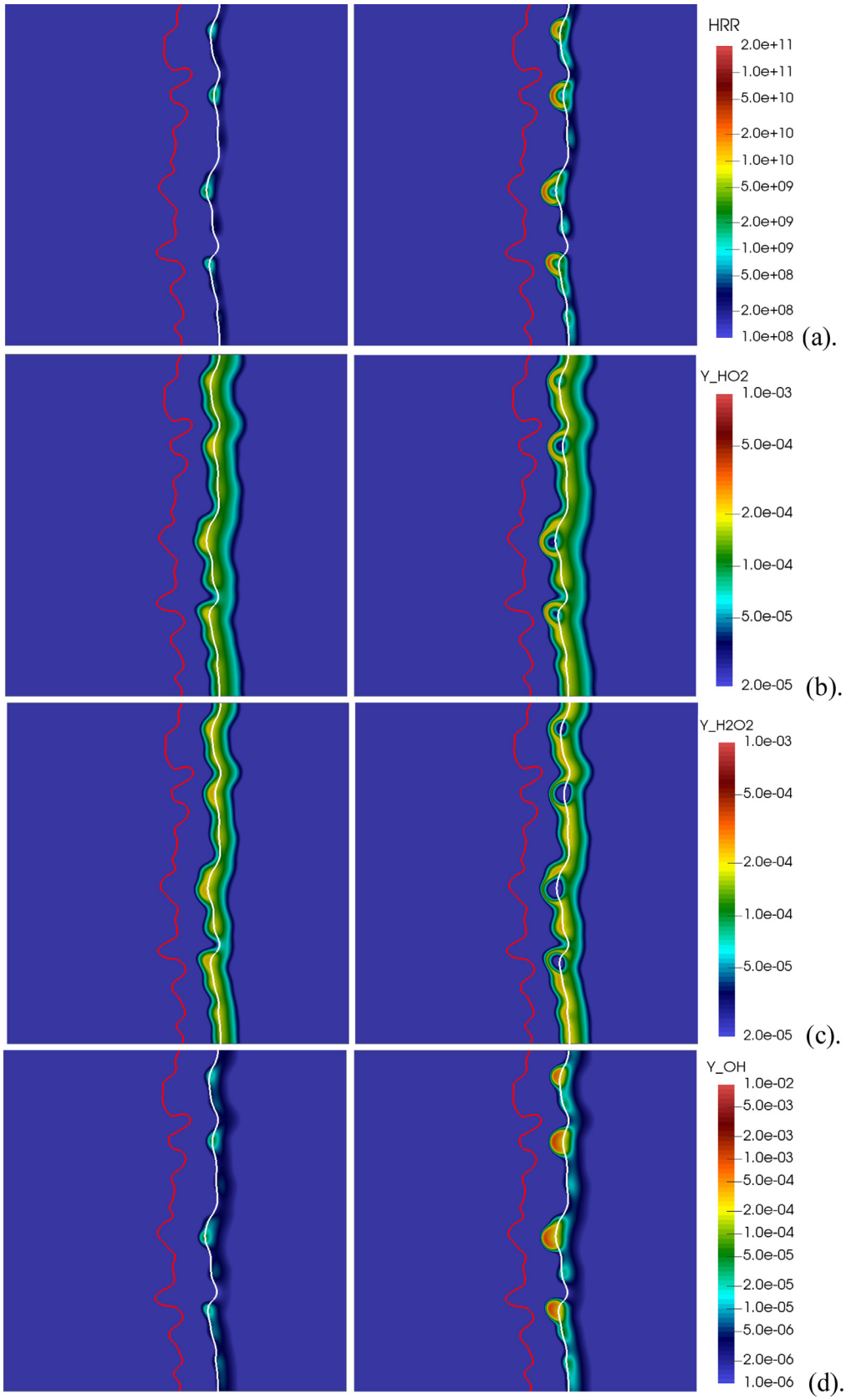

Fig. 10. Turbulent calculation: instantaneous radicals and heat release rate contours at the ignition time for $p = 5$ atm (a) Heat release rate (b) HO_2 (c) H_2O_2 (d) OH. (For interpretation of the references to colour in this figure text, the reader is referred to the web version of this article.)

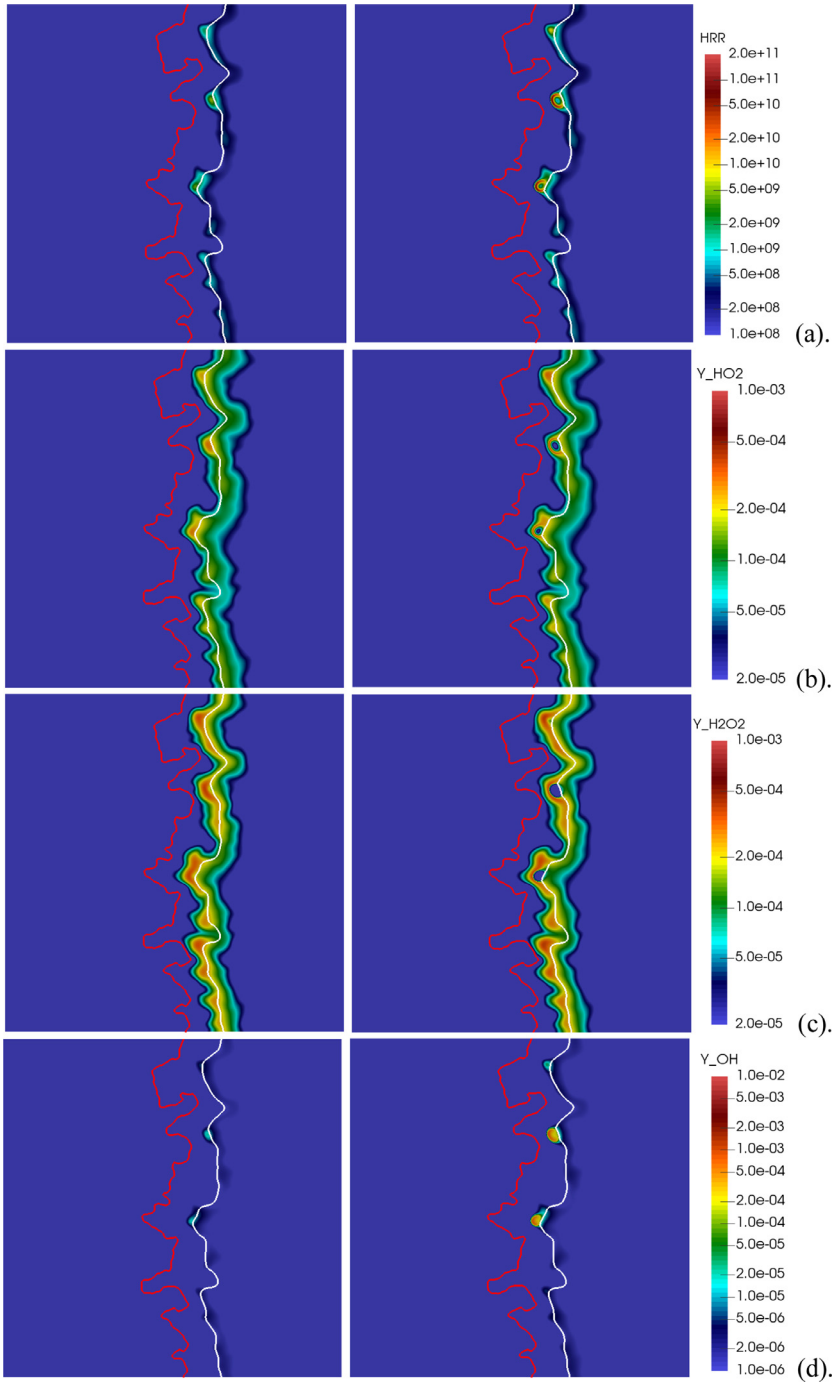

Fig. 11. Turbulent calculation: instantaneous radicals and heat release rate contours at the ignition time $t = 3.80$ (left side) and $t = 3.90$ (right side) for $p = 10$ atm. (a) Heat release rate (b) HO_2 (c) H_2O_2 (d) OH. (For interpretation of the references to colour in this figure text, the reader is referred to the web version of this article.)

with dash lines in Fig. 8(b). Concentration of H_2O_2 shows similar behaviour with HO_2 in Fig. 7(b).

4.3. Turbulent mixing ignition

Turbulent mixing ignitions (TMI) are performed under different pressures. Contours of instantaneous heat release rate and mass fraction of HO_2, H_2O_2 and OH are shown in Figs. 9–12. The isolines of most reactive mixture fraction (white lines) and stoichiometric mixture fraction (red lines) are also shown in the figures. Auto-ignition occurs on the most reactive isolines and are away from the stoichiometric mixture fraction isolines for all cases of different pressures. IDTs for different pressures of $p = 1$, 5, 10, 30 atm are 0.28, 1.7, 3.8, 4.72 ms respectively.

4.3.1. p = 1 atm at the ignition time t = 0.28 and t = 0.29 ms

In the presence of weak turbulence at $p = 1$ atm in Fig. 9, ignition occurred uniformly in the most reactive region. The ignition region is wide for $p = 1$ atm, for the same reason indicated in LMI. In Fig. 9(b), HO_2 mainly distributes on the cold side of the ignition zone. In Fig. 9(d), OH distributes in the center of the ignition zone. Moreover, concentrations of H_2O_2 are trivial under $p = 1$ atm and not shown here. After all, ignition process shows similar features as LMI.

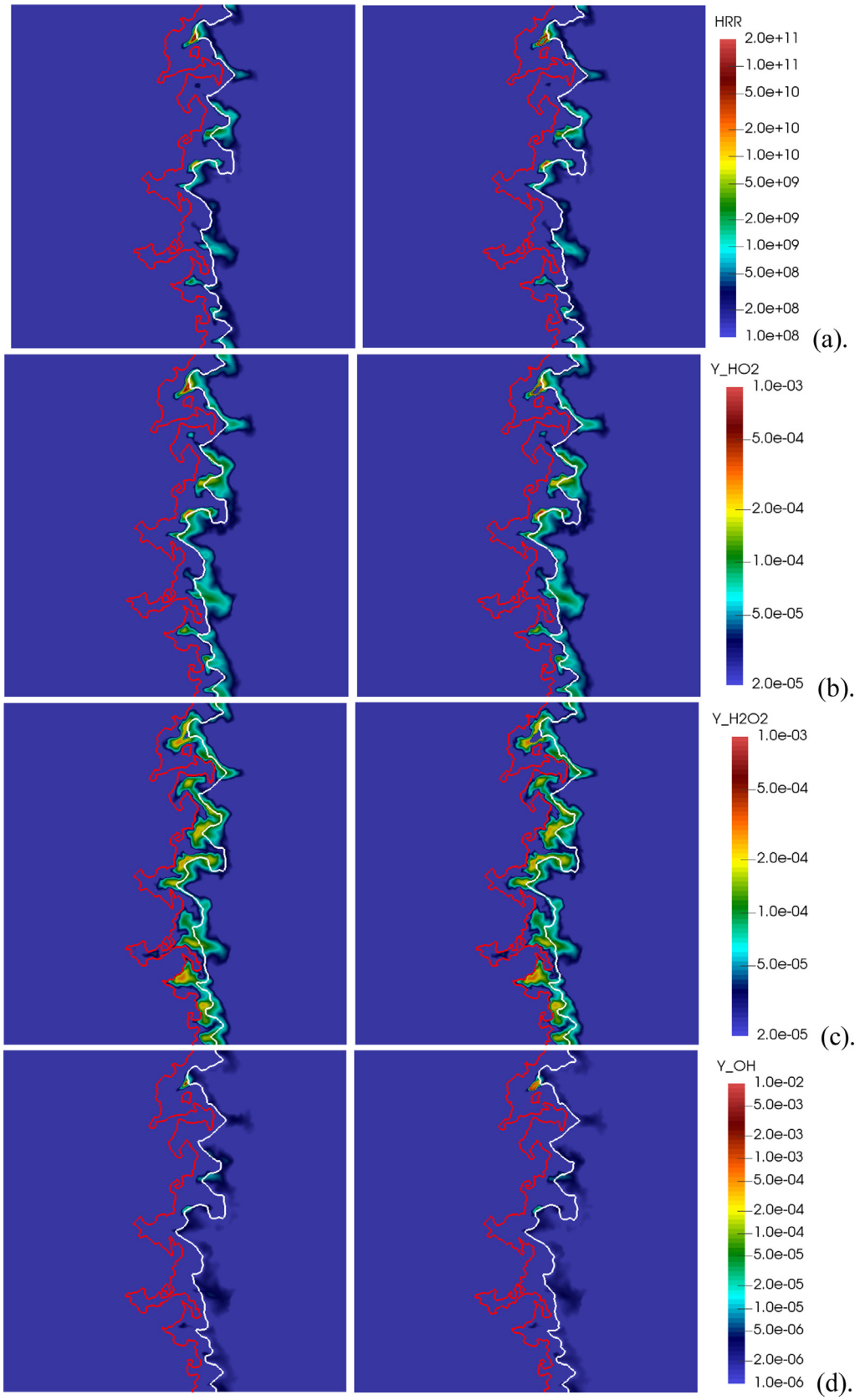

Fig. 12. Turbulent calculation: instantaneous radicals and heat release rate contours at the ignition time for $p = 30$ atm (a) Heat release rate (b) HO_2 (c) H_2O_2 (d) OH. (For interpretation of the references to colour in this figure text, the reader is referred to the web version of this article.)

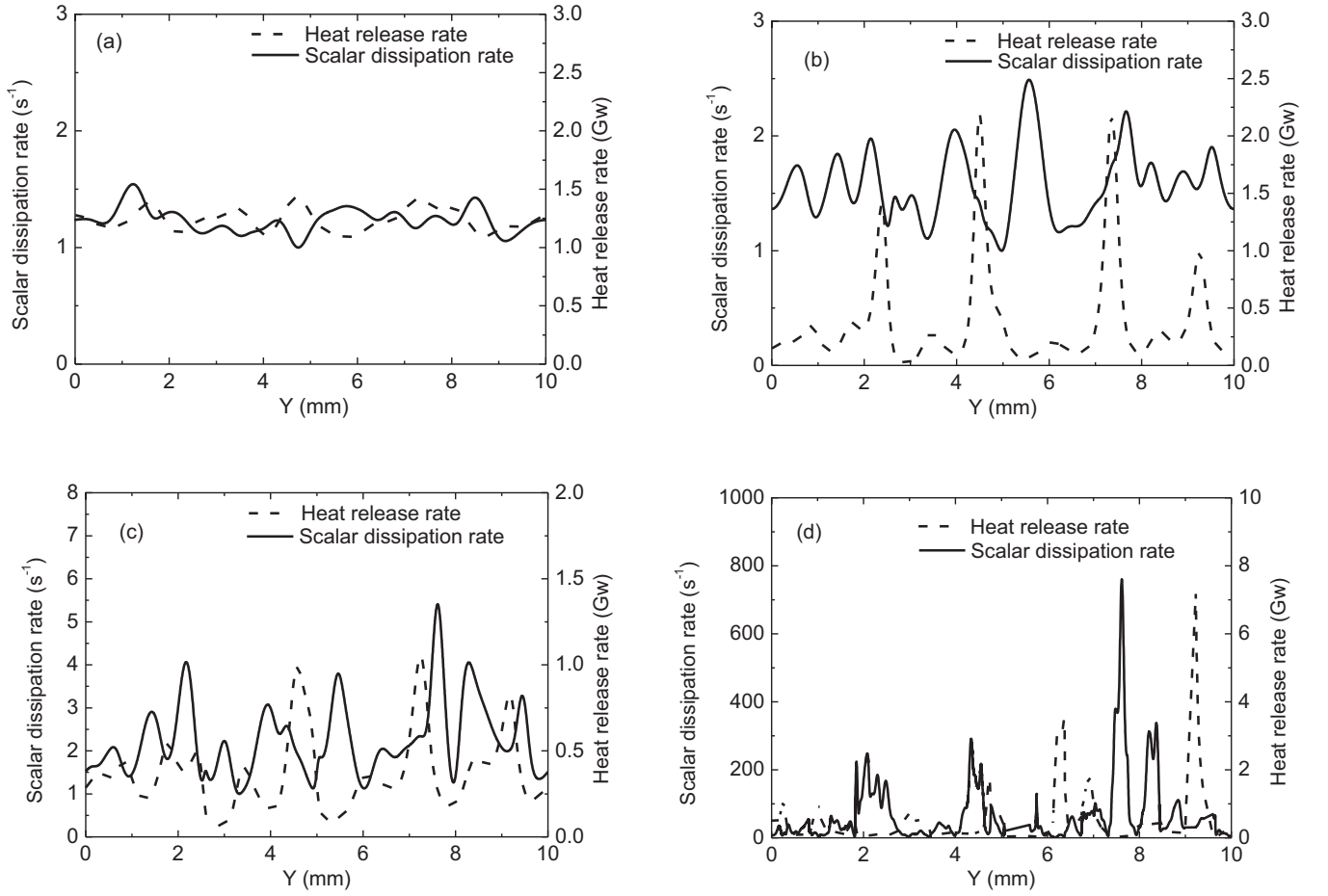

Fig. 13. Conditional heat release rate profile and scalar dissipation rate profile as a function of *Y*-axis along the most reactive mixture fraction isoline at ignition instant under various pressures (a) $p = 1$ atm, $t = 0.28$ ms (b) $p = 5$ atm, $t = 1.70$ ms (c) $p = 10$ atm, $t = 3.80$ ms (d) $p = 30$ atm, $t = 4.72$ ms.

4.3.2. p = *5 atm at the ignition time* t = *1.70 and* t = *1.80 ms*

As pressure increases to $p = 5$ atm in Fig. 10, ignition spots become scattered. After ignition, the flame kernels propagate to the fuel rich zones. The flame propagation is like a 'half-spherical' flame in the mixing layer zone. As temperature increases on the lean side, the wrinkling of the most reactive mixture fraction isoline (white line) is less than that of stoichiometric mixture fraction isoline (red line) with viscosity increasing. Flame fronts are barely winkled by the turbulence. Heat release focuses on the flame front on the rich side of the kernel.

4.3.3. p = *10 atm at the ignition time* t = *3.80 ms and* t = *3.90 ms*

It can be seen in Fig. 11 that ignition process of $p = 10$ atm is similar to that of $p = 5$ atm. Several ignition spots emerge on the most reactive mixture fraction isoline (white line) at the ignition time $t = 3.80$ ms. In Fig. 11(a), at $t = 3.90$ ms, heat release rate at the center of the ignition spots drops dramatically as the depletion of the reactants. In addition, the ignition spot transit to a flame front on the edge of the ignition spots. In Fig. 11(b) and (c), HO_2 and H_2O_2 peaks in the ignition spots at the ignition time instant and drops after the transition. In Fig. 11(d), concentrations of OH are trivial in the ignition spots and increases on the flame front, which contributes to the successful transition of ignition to flame propagation.

4.3.4. p = *30 atm at the ignition time* t = *4.72 and* t = *4.80 ms*

In Fig. 12, as pressure increases, mixture fraction isolines are more wrinkled and fractal ignition spots are observed for the smaller turbulent length scale. At the ignition instant $t = 4.72$ ms, ignition spots are located on the most reactive mixture isoline of 0.1 (white line), which is consistent with the LMI calculations. HO_2 and H_2O_2 can still be used as a good marker variable for identification of ignition spots. Although turbulent Reynolds numbers are identical for all pressures, high dissipation rates at $p = 30$ atm interrupt the continuity of the ignition along the most reactive mixture fraction line, which leads to distributed and stretched ignition spots. The ignition spots are more irregular for $p = 30$ atm.

4.3.5. The effects of fluctuations of scalar dissipation rate

The relationship between scalar dissipation rate and heat release rate along the most reactive isoline at ignition time under different pressures is shown in Fig. 13. For all cases, the regions with lower scalar dissipation rate correspond to higher heat release rate, which indicates the locations of auto-ignition spots along the most reactive mixture fraction isoline. High dissipation decelerates the thermal runaway stage through heat loss from the ignition spots, and low dissipation rate accelerates thermal runaway. In Fig. 13(a), at $p = 1$ atm, heat release rate ranges from 1 Gw to 1.4 Gw along the *Y*-axis, which indicates uniformly ignition at $p = 1$ atm. In Fig. 13(b) and (c), at $p = 5$ atm and 10 atm, the range of heat release rate becomes large, and there are regions where heat release rates are too small to ignite the mixtures. This indicates scattered ignition spots in the domain. In Fig. 13(d), at $p = 30$ atm, magnitude and frequency of the fluctuations of scalar dissipation rate are larger than other cases. There are two sharp

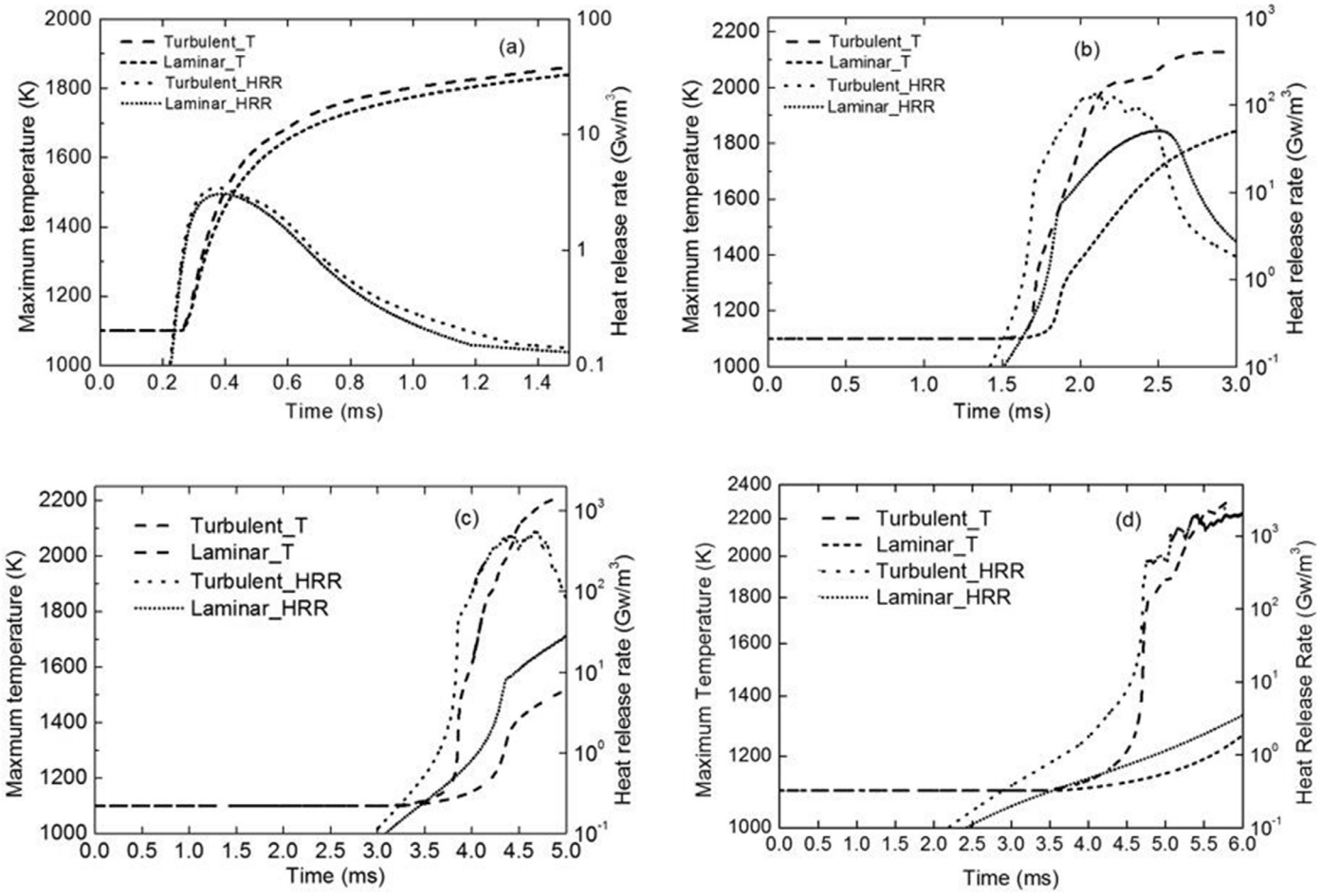

Fig. 14. Evolution of maximum temperature and heat release rate in the auto-ignition of laminar and turbulent diffusion mixing layer under different pressures (a) $p = 1$ atm (b) $p = 5$ atm (c) $p = 10$ atm (d) $p = 30$ atm.

increasing in heat release rate where scalar dissipation rates are relatively low.

4.4. Comparison of ignition characteristics between LMI and TMI

Fig. 14 shows the evolution of maximum temperature and heat release rate in the computational domain of laminar and turbulent diffusion mixing layer under different pressures. As indicated earlier, auto-ignition process can be divided into two stages, which are induction stage and thermal runaway stage. It can be seen that the induction times are almost identical for laminar and turbulent cases for all cases. Turbulence has little influence on the induction time but significant influence on thermal runaway, which leads to a shorter ignition delay time for the turbulent cases. As the temperature increase and heat release of the thermal runaway stage are linear to residence time, turbulence will create lower dissipation rate zones that will accelerate thermal runaway. However, induction stage is characterized by radical explosion exponentially, and the induction time is barely affected by turbulence.

5. Conclusions

DNS of hydrogen-air mixing layer auto-ignition is performed in HMI, LMI, TMI. Different pressures $p = 1$, 5, 10, 30 atm on ignition characteristics are investigated. Results in the present work confirm qualitatively theoretical and experimental findings from literature regarding the correlation between the ignition spots and most reactive mixture fraction. Previous studies of hydrogen/air mixing layer focus on lower pressures $p = 1$ atm. The ignition chemistry lies in the first ignition regime. In the present work, the pressure has been extended to $p = 5$,10 and 30 atm in second and third ignition regime. Several conclusions can be drawn from the present study.

- For most reactive mixture fractions are defined as the locations of ignition spots in the mixture fraction space. Most reactive mixture fractions in diffusion auto-ignition are inconsistent with HMI calculations and shift to the rich side owing to diffusion for all pressures. Most reactive mixture fractions in TMI are identical to LMI. Therefore, calculations performed by LMI can be used as indications for TMI.
- At elevated pressures, auto-ignition chemistry is different from low pressures. The importance of H_2O_2 and HO_2 is highlighted as radical sinks during the ignition process. The location of peak HO_2 and H_2O_2 always remains at low temperatures. When ignition happens in the local spots, HO_2 and H_2O_2 are consumed quickly. Thus, HO_2 can also be used as an indicator for locating the ignition spots. After ignition, OH radicals increase dramatically on the edge of ignition spots. Therefore, OH radicals can be used as a marker variable for the transition of auto-ignition to flame propagation, and global ignition capability at elevated pressures of the second and third ignition zone.
- Auto-ignition of diffusion mixing layers consists of radical explosion and thermal runaway. At high pressures, scalar dissipation has little influence on the radical explosion stage for the exponential accumulation of the radicals. However, turbu-

lence has great influence on the thermal runaway and accelerates ignition through promoting thermal runaway. As pressures increasing, magnitude and frequency of the fluctuations of scalar dissipation rate become larger, resulting to sharp increasing in heat release rate where scalar dissipation rates are relatively low.

Acknowledgements

Support from the Natural Science Foundation of China (Grant No. 91441120) and the Centre for Combustion Energy at Tsinghua University is gratefully acknowledged. The simulations were performed on ARCHER funded under the EPSRC projects “UK Consortium on Mesoscale Engineering Sciences (UKCOMES)” (Grant No. EP/L00030X/1) and “High Performance Computing Support for United Kingdom Consortium on Turbulent Reacting Flow (UKCTRF)” (Grant No. EP/K024876/1).

References

[1] Stenlåås O, Christensen M, Egnell R, Johansson B, Mauss F. Hydrogen as homogeneous charge compression ignition engine fuel, SAE Tech Pap, 2004.
[2] Wang S, Ji C, Zhang B, Liu X. Realizing the part load control of a hydrogen-blended gasoline engine at the wide open throttle condition. Int J Hydrog Energy 2014;39:7428–36.
[3] Aliyu M, Nemitallah MA, Said SA, Habib MA. Characteristics of H_2-enriched CH_4-O_2 diffusion flames in a swirl-stabilized gas turbine combustor: experimental and numerical study. Int J Hydrog Energy 2016;41:20418–32.
[4] Sanchez AL, Balakrishnan G, Linan A, Williams FA. Relationships between bifurcation and numerical analyses for ignition of hydrogen-air diffusion flames. Combust Flame 1996;105:569–90.
[5] Kreutz TG, Law CK. Ignition in nonpremixed counterflowing hydrogen versus heated air: computational study with detailed chemistry. Combust Flame 1996;104:157–75.
[6] Lee D, Hochgreb S. Hydrogen autoignition at pressures above the second explosion limit (0.6–4.0MPa). Int J Chem Kinet 1998;30:385–406.
[7] Veynante D, Vervisch L. Turbulent combustion modeling. Prog Energy Combust Sci 2002;28:193–266.
[8] Candel S, Thévenin D, Darabiha N, Veynante D. Progress in numerical combustion. Combust Sci Technol 1999;149:297–337.
[9] Echekki T, Chen JH. Direct numerical simulation of autoignition in non-homogeneous hydrogen-air mixtures. Combust Flame 2003;134:169–91.
[10] Echekki T, Chen JH. High-temperature combustion in autoigniting non-homogeneous hydrogen/air mixtures. Proc Combust Inst 2002;29:2061–8.
[11] Mastorakos E. Ignition of turbulent non- premixed flames. Prog Energy Combust Sci 2009;35:57–97.
[12] Hilbert R, Tap F, Veynante D, Thevenin D. A new modeling approach for the autoignition of a non-premixed turbulent flame using DNS. Proc Combust Inst 2002;29:2079–85.
[13] Lipatnikov AN, Chomiak J. Turbulent flame speed and thickness: phenomenology, evaluation, and application in multi-dimensional simulations. Prog Energy Combust Sci 2002;28:1–74.
[14] Hilbert R, Thevenin D. Influence of differential diffusion on maximum flame temperature in turbulent nonpremixed hydrogen/air flames. Combust Flame 2004;138:175–87.
[15] Im HG, Chen JH, Law CK. Ignition of hydrogen-air mixing layer in turbulent flows. Symp (Int) Combust 1998;27:1047–56.
[16] Hilbert R, Thévenin D. Autoignition of turbulent non-premixed flames investigated using direct numerical simulations. Combust Flame 2002;128:22–37.
[17] Thévenin D, Behrendt F, Maas U, Przywara B, Warnatz J. Development of a parallel direct simulation code to investigate reactive flows. Comput Fluids 1996;25:485–96.
[18] Thévenin D, Fru G, Janiga G. Direct numerical simulations of the impact of high turbulence intensities and volume viscosity on premixed methane flames. J Combust 2011.
[19] Fru G, Thévenin D, Markus D. Direct numerical simulations of turbulent H2-Air pre-mixtures and analysis towards safety-relevant ignition prediction. Direct Large-Eddy Simul 2015:525–31 IX.
[20] Fru G, Thevenin D, Janiga G. Impact of turbulence intensity and equivalence ratio on the burning rate of premixed methane-air flames. Energies 2011;4:878–93.
[21] Honein AE, Moin P. Higher entropy conservation and numerical stability of compressible turbulence simulations. J Comput Phys 2004;201:531–45.
[22] Baum M, Poinsot T, Thévenin D. Accurate boundary conditions for multicomponent reactive flows. J Comput Phys 1995;116:247–61.
[23] Poinsot T, Lele S. Boundary conditions for direct simulations of compressible viscous flows. J Comput Phys 1992;101:104–29.
[24] Ranga Dinesh KKJ, Jiang X, van Oijen JA. Direct numerical simulation of non-premixed syngas burning with detailed chemistry. Fuel 2013;107:343–55.
[25] Ranga Dinesh KKJ, Jiang X, van Oijen JA. Hydrogen-enriched non-premixed jet flames: compositional structures with near-wall effects. Int J Hydrog Energy 2013;38:5150–64.
[26] Ranga Dinesh KKJ, Jiang X, van Oijen JA, Bastiaans RJM, de Goey LPH. Hydrogen-enriched nonpremixed jet flames: effects of preferential diffusion. Int J Hydrog Energy 2013;38:4848–63.
[27] Ranga Dinesh KKJ, Shalaby H, Luo KH, van Oijen JA, Thévenin D. Effects of pressure on cellular flame structure of high hydrogen content lean premixed syngas spherical flames: a DNS study. Int J Hydrog Energy 2016;41:21516–31.
[28] Ranga Dinesh KKJ, Shalaby H, Luo KH, van Oijen JA, Thévenin D. Heat release rate variations in high hydrogen content premixed syngas flames at elevated pressures: Effect of equivalence ratio. Int J Hydrog Energy 2017;42:7029–44.
[29] Maas U, Warnatz J. Ignition processes in hydrogen-oxygen mixtures. Combust Flame 1988;74:53–69.
[30] Bilger RW. The structure of turbulent nonpremixed flames. Symp (Int) Combust 1989;22:475–88.
[31] Yu R, Bai XS. Direct numerical simulation of lean hydrogen/air auto-ignition in a constant volume enclosure. Combust Flame 2013;160:1706–16.
[32] Lutz AE, Kee RJ, Miller JA. SENKIN: A FORTRAN program for predicting homogeneous gas phase chemical kinetics with sensitivity analysis. Sandia National Laboratories Report SAND-87-8248; 1988.